Characteristics of Ar^+-ion-implanted Amorphous-IGZO

Keisuke YASUTA*, Toshimasa UI, Yuya YAMANE, Toshihiko SAKAI, Yasunori ANDOH, and Junichi TATEMICHI

Nissin Ion Equipment Co., Ltd. conducted research on electron transport properties of an argon-ion-implanted amorphous InGaZnO (a-IGZO) film deposited on a glass substrate. The research obtained valuable data on electron concentration and Hall mobility of the film at various depths from the surface. The result shows that the a-IGZO film has a high electron concentration in deep regions compared with an argon plasma-treated a-IGZO film. In addition, the company estimated the argon stopping powers of a-IGZO and the donor level of 0.05-0.1 eV below conduction band bottom energy, which can be applied to resistance control for a-IGZO device processing.

Keywords: flat-panel display (FPD), oxide semiconductor, IGZO, ion implantation

1. Introduction

In the next-generation electronics field for flat-panel displays (FPDs), research and development on amorphous InGaZnO (a-IGZO), which is characterized by a wide band gap, transparency, flexibility, and excellent film thickness uniformity, have been widely conducted.

a-IGZO thin-film transistors (TFTs) fabricated in the vacuum process achieve high-speed operation, low power consumption, and high breakdown voltage.(1),(2) Thus, a-IGZO TFTs are expected to be applied to next-generation FPDs, such as flexible displays, transparent displays, and low-power-consumption displays. To improve the performance of the oxide semiconductor TFTs, technologies to lower the resistance in the source/drain regions by plasma irradiation,(3) excimer laser irradiation,(4) and ion implantation(5),(6) have been studied. Of these technologies, ion implantation has superb advantages in terms of depth direction controllability, microfabrication performance, and productivity. As the technology is expected to further improve the performance and achieve a higher definition of displays, Nissin Ion Equipment Co., Ltd. has been conducting research and development focusing on this field.

Previously, Nissin Ion Equipment reported that oxygen vacancy (Vo) generated by noble gas ion implantation contributed to reducing the sheet resistance R_s of the a-IGZO oxide semiconductor.(7),(8) However, the concentration of noble gas implanted in an a-IGZO film is low, and the ionization cross-section is small. Thus, it is difficult to measure the concentration distribution of noble gas elements and Vo in a-IGZO films.

To estimate electron transport properties and establish resistance value control technology for a-IGZO films, we performed one of the conventional noble-gas ion Ar^+ implantation and Ar plasma irradiation for comparison. We also estimated the stopping power of a-IGZO films for Ar and the donor level based on the obtained results.

2. Experiment Procedure and Results

2-1 Sheet resistance evaluation of Ar^+-implanted and Ar-plasma-irradiated a-IGZO films

a-IGZO thin films with a film thickness 50 nm and sheet resistance ~ 10^{12} Ω/sq. were formed on glass substrates whose thickness was 0.5 mm by inductively coupled plasma sputtering (gas flow rate: Ar/O = 95/5 sccm, pressure: 0.9 Pa, RF power: 7 kW, target: $InGaZnO_4$, target voltage: −400 V).(9) To reduce R_s, an ion implanter(10) of Nissin Ion Equipment was used to implant Ar^+ ions (ion energy: E_{ion} 20–80 keV, dose: 1 × 10^{15} ions/cm^2). For comparison, Ar plasma irradiation was also performed (pressure: 20 Pa, RF power: 10–30 W, processing time: 1–10 min). To compare thermal stability, heat treatment was performed in the atmosphere at 300°C for 1 h after Ar^+ ion implantation or Ar plasma irradiation.

Figure 1 (a) shows the E_{ion} dependence of R_s of a-IGZO films after Ar^+ ion implantation and after heat treatment at 300°C following ion implantation. After ion implantation, R_s of a-IGZO films decreased to 3 × 10^3–1 × 10^4 Ω/sq. Meanwhile, heat treatment at 300°C after ion implantation increased R_s to 1 × 10^4–2 × 10^6 Ω/sq. Both after ion implantation and after heat treatment at 300°C, R_s was a decreasing function of E_{ion} and the E_{ion} dependence of R_s was high after heat treatment in particular.

Figure 1 (b) shows the RF power dependence of R_s of a-IGZO films after Ar plasma irradiation and after heat treatment at 300°C following plasma irradiation. After plasma irradiation, R_s of a-IGZO films decreased to ~ 2 × 10^3 Ω/sq. regardless of the plasma irradiation condition. Meanwhile, heat treatment after plasma irradiation increased R_s to 1 × 10^6–1 × 10^7 Ω/sq. regardless of the irradiation condition.

The results above suggest the following. In the case of Ar plasma irradiation, Vo, which supplies electrons, is generated near the surface of a-IGZO films and easily decreases due to the reaction with O_2 and H_2O in the atmosphere. Meanwhile, in the case of Ar^+ ion implantation, Vo is generated in deep regions away from the surface, which are unlikely to be affected from the surface. This ensures high thermal stability.

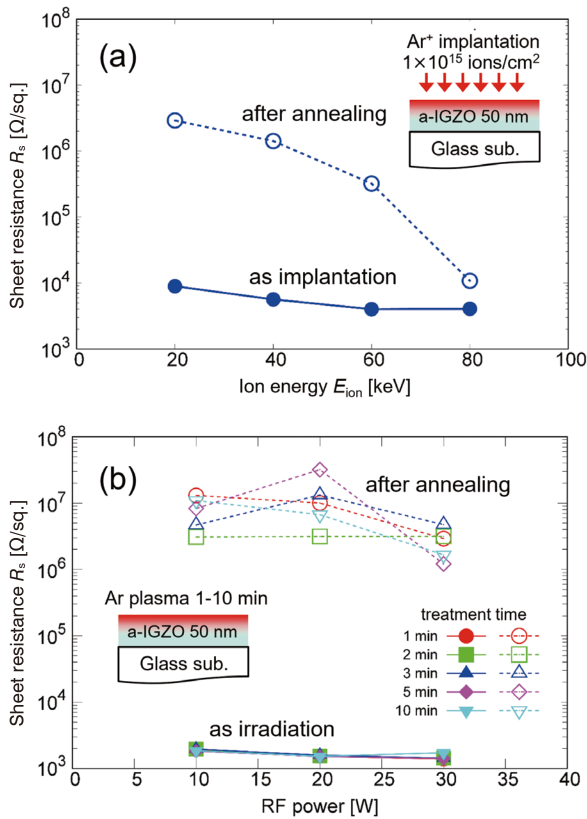

Fig. 1. (a) Ion energy E_{ion} dependence and (b) RF power dependence of the a-IGZO film sheet resistance R_s before and after heat treatment at 300°C (Figure 2 of the published paper[8] (copyright: FTFMD 2021))

2-2 Depth direction analysis of the electron transport properties

To clarify the difference in thermal stability between Ar^+ ion implantation and Ar plasma irradiation, the electron transport properties were analyzed in the depth direction by combining wet etching and Hall measurement.

Figure 2 shows an overview of the depth direction analysis of electron transport properties of a-IGZO films. Ar^+ ion implantation (80 keV, 1×10^{15} ions/cm^2) or Ar plasma irradiation (20 Pa, 30 W, 10 min) was performed on the a-IGZO film (thickness: 170 nm)/glass substrate structure. Isolation and ohmic electrode formation were conducted to fabricate a Hall measurement device. Figure 3 shows sheet electron density n_s, Hall mobility μ, and R_s as a function of etching depth from the surface of a-IGZO films, which were obtained by repeating the process of wet etching, film thickness measurement by spectroscopic ellipsometry, and Hall measurement. n_s of Ar-plasma-irradiated a-IGZO films significantly decreased as the increase in the etching depth, which indicates almost all of Vo were generated near the surface of a-IGZO films. Meanwhile, compared to the results of Ar plasma irradiation, n_s and μ of Ar^+-implanted a-IGZO films decreased gradually as the increase in the etching depth. This result

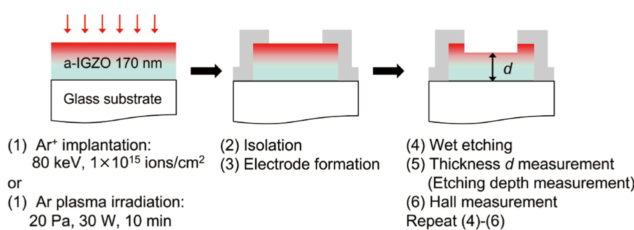

Fig. 2. Overview of the depth direction analysis of a-IGZO films after Ar^+ ion implantation and Ar plasma irradiation (Figure 1 of the published paper[8] (copyright: FTFMD 2021))

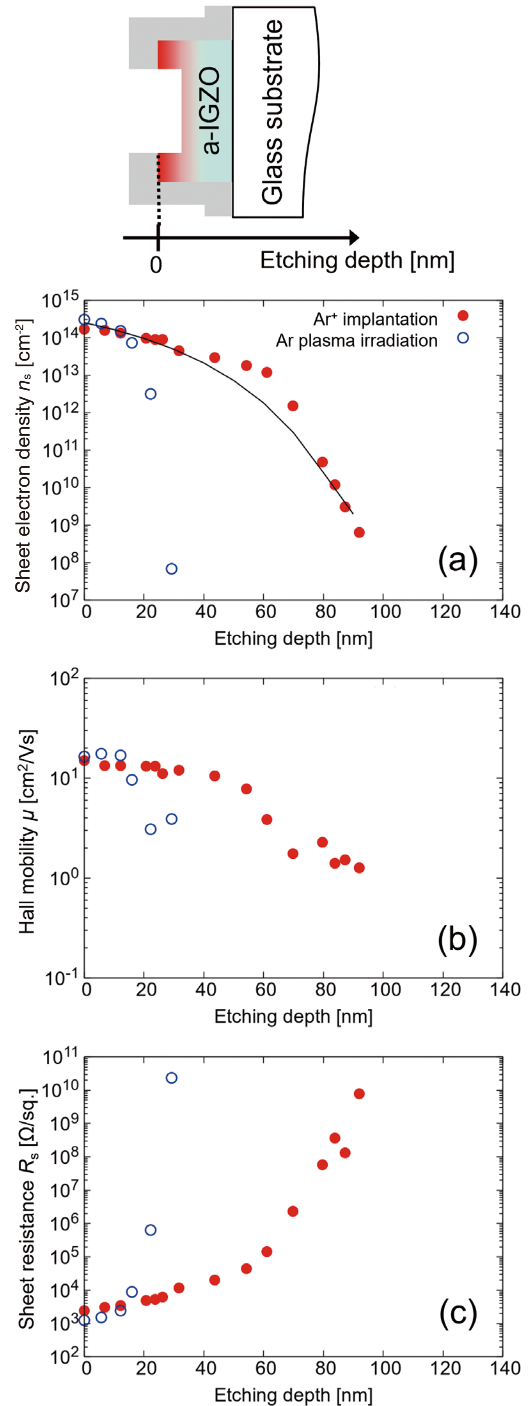

Fig. 3. Relationship between (a) sheet electron density n_s, (b) Hall mobility μ, and (c) sheet resistance R_s and the etching depth of a-IGZO films after Ar^+ ion implantation and Ar plasma irradiation (Figure 3 of the published paper[8] (copyright: FTFMD 2021))

shows that high-density Vo was generated into deep regions from the surface of a-IGZO films.

To evaluate the electron transport properties in the depth direction more quantitatively, the parallel conductance model, which is shown in Fig. 4, was used to calculate the depth direction profile of local electron density n_j and local Hall mobility μ_j in a-IGZO films. In this model, the electrical conductivity of electrons is described by the synthesis of parallel connection of each layer. When the weak magnetic field approximation ($\mu B << 1$) holds, the two equations below hold given the parallel conductance Hall coefficient.

$$\sigma_{\mathrm{meas}} \simeq \sum_j \sigma_j \quad (\sigma_{\mathrm{meas}} = n_{\mathrm{meas}} \cdot \mu_{\mathrm{meas}},\ \sigma_j = n_j \cdot \mu_j) \cdots (1)$$

$$\sigma_{\mathrm{meas}} \cdot \mu_{\mathrm{meas}}^2 \simeq \sum_j \sigma_j \cdot \mu_j^2 \cdots\cdots (2)$$

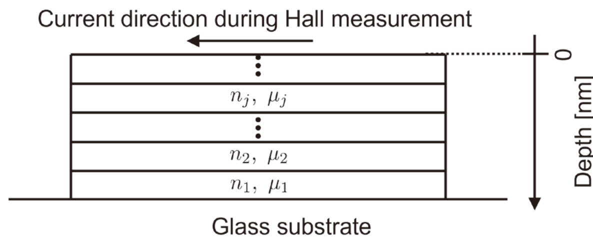

Fig. 4. Parallel conductance model
(Figure 4 of the published paper[8] (copyright: FTFMD 2021))

Here, based on the results in Fig. 3, the weak magnetic field approximation holds given that the Hall mobility of a-IGZO films is μ = 1–10 cm²/Vs and the magnetic flux density B is ~ 0.5 T. σ_{meas}, n_{meas}, and μ_{meas} are conductance, electron density, and Hall mobility, respectively, obtained in the Hall measurement. Thus, n_j and μ_j of each section can be estimated by using Eqs. (1) and (2).

Figure 5 shows the depth direction profile of n_j and μ_j obtained through calculation. Depth 0 corresponds to the a-IGZO film surface. the electron density is high in regions of 0–20 nm for Ar-plasma-irradiated films and in regions of 0–60 nm for Ar^+-ion-implanted films. Given that Ar does not serve as a donor, on the assumption that only Vo generates electrons, the Vo profile can be estimated using a simulator (Transport of Ions in Matter, TRIM[11]) based on the n_j profile. Here, the Vo profile in Fig. 5 almost matches the n_j profile. Based on these correlations, the ion energy dependence of electronic and nuclear stopping power of the a-IGZO films for Ar were obtained as shown in Fig. 6. Here, the bond energy of In, Ga, Zn, and O is 2–3 eV.[12],[13] We also estimated the depth direction profile of Ar atoms implanted in the a-IGZO films by using the stopping power obtained.

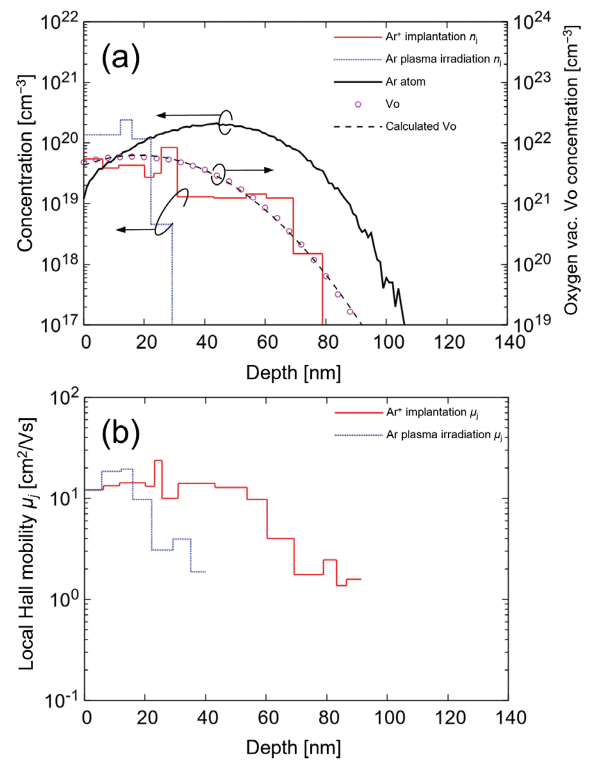

Fig. 5. Depth direction profile of (a) local electron density n_j and (b) local Hall mobility μ_j
(Figure 5 of the published paper[8] (copyright: FTFMD 2021))

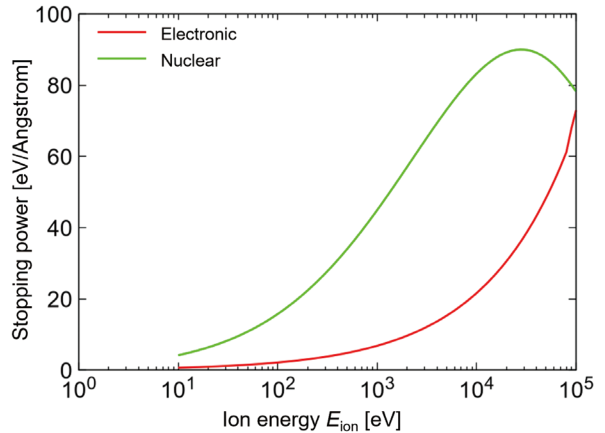

Fig. 6. Ion energy E_{ion} dependence of the electronic and nuclear stopping power of the a-IGZO film for Ar
(Figure 6 of the published paper[8] (copyright: FTFMD 2021))

2-3 Elucidation of the Vo donor level

To determine the Vo donor level, Poisson-Schrödinger calculation[14] was performed. The calculation flow is shown in Fig. 7. The energy band profile and the electron distribution at 300 K shown in Fig. 8 were obtained based on the Vo fitting line, which was obtained through the calculation shown in Fig. 5, and the assumption that two electrons were generated by each Vo. Here, E_c is the energy at the bottom of the conduction band, E_v is the energy at the top of the valence band, E_D is the mean Vo-donor-level, E_F is the Fermi energy, ρ is the electron density, and d is the

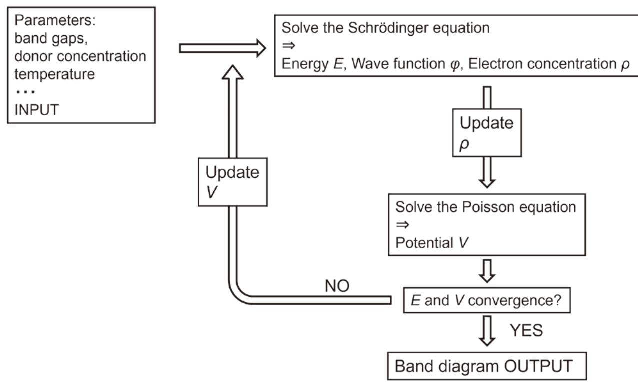

Fig. 7. Poisson-Schrödinger calculation flow

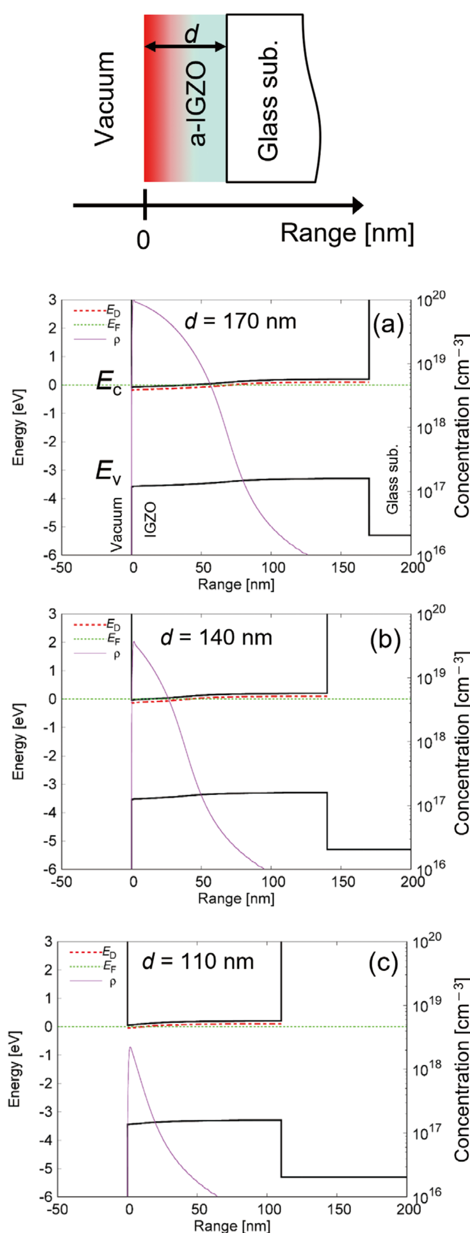

Fig. 8. Examples of energy band profiles and electron distributions at 300 K in the a-IGZO/glass substrate structure obtained by calculation (Figure 7 of the published paper[8] (copyright: FTFMD 2021))

film thickness shown in Fig. 2. The band gaps of the a-IGZO films and glass substrates were ~ 3.5 eV and ~ 8.4 eV, respectively.[7]

Based on the calculation, the donor level $E_c - E_D$ = 0.05–0.1 eV was obtained. As shown in Fig. 3, n_s (solid line) obtained through the calculation well matches the experiment results. This shows the validity of the calculation.

3. Conclusion

We investigated the properties of Ar^+-ion-implanted and Ar-plasma-irradiated a-IGZO films on glass substrates. By combining the Hall measurement with wet etching, the depth direction profile of local electron density and local Hall mobility was obtained based on the depth direction information of electron transport properties. It was found that Ar^+ ion implantation generated high-density electrons, which were induced by Vos, at deep positions from the a-IGZO film surface, achieving high thermal stability. We also estimated the stopping power of a-IGZO against Ar and the donor level at positions of 0.05–0.1 eV from the bottom of the conduction band. These findings are useful for ion implantation-based resistance value control technology for the a-IGZO device process.

References

(1) K. Nomura, H. Ohta, A. Takagi, T. Kamiya, M. Hirano, and H. Hosono, Nature 432 (2004) 488
(2) T. Kamiya, K. Nomura, and H. Hosono, J. Disp. Technol. 5 (2009) 273
(3) H. Jeong, B. Lee, Y. Lee, J. Lee, M. Yang, I. Kang, M. Mativenga, and J. Jang, Appl. Phys. Lett. 104 (2014) 022115
(4) M. Nakata, H. Tsuji, Y. Fujisaki, H. Sato, Y. Nakajima, T. Takei, T. Yamamoto and T. Kurita, Appl. Phys. Lett. 103 (2013) 142111
(5) R. Chowdhurya, M. Kabirb, R. Manleyc, and K. Hirschman, ECS Transactions 92 (2019) 135
(6) L. Qian, W. Tang and P. Laia, ECS Solid State Lett. 3 (2014) 87
(7) T. Ui, R. Fujimoto, T. Sakai, D. Matsuo, Y. Setoguchi, Y. Andoh, and J. Tatemichi, the 27th AM-FPD '20 (2020) 115
(8) K. Yasuta, T. Ui, T. Ikeda, D. Matsuo, T. Sakai, S. Dohi, Y. Setoguchi, E. Takahashi, Y. Andoh, and J. Tatemichi, the 28th AM-FPD (2021) 77
(9) D. Matsuo, R. Miyanaga, T. Ikeda, S. Kishida, Y. Setoguchi, Y. Andoh, M. N. Fujii, and Y. Uraoka, the 25th IDW '18, FMCp7 - 2L (2018) 560.
(10) S. Dohi, H. Kai, T. Nagao, T. Matsumoto, M. Onoda, K Nakao, Y. Inouchi, J. Tatemichi, and M. Nukayama, The Nissin Electric Review 62 (2017) 17
(11) J. Ziegler and J. Biersack, Stopping Power and Range of Ion in Matter (2008)
(12) K. Takechi, Y. Kuwahara, J. Tanaka, and H. Tanabe, Jpn. J. Appl. Phys. 58 (2019) 038005
(13) H.-W. Park, J. Bae, H. Kang, D. H. Kim, P. Jung, H. Park, S. Lee, J. U. Bae, S. Y. Yoon, I. Kang, SID Symposium Digest of Technical Papers, 50 (2019) 1222
(14) G. L. Snider, Computer Program 1D Poisson/Schrödinger: A Band Diagram Calculator (University of Notre Dame, Notre Dame, Indiana (1995)

Contributors

The lead author is indicated by an asterisk (*).

K. YASUTA*
• Nissin Ion Equipment Co., Ltd.

T. UI
• Ph.D.
Nissin Ion Equipment Co., Ltd.

Y. YAMANE
• Nissin Ion Equipment Co., Ltd.

T. SAKAI
• Nissin Electric Co., Ltd., Manager

Y. ANDOH
• Ph.D.
Fellow
Nissin Electric Co., Ltd.

J. TATEMICHI
• Nissin Ion Equipment Co., Ltd.
Executive Engineer

This paper is based on the paper (the 28th AM-FPD, 2021, 77), and the copyrights of the contents cited from the paper are attributed to the International Society of Functional Thin Film Materials & Devices.
This paper is also based on the Nissin Electric Review vol. 68.